



Research Article

Numerical evaluation of prestressed concrete slabs subjected to impact loading

R. Tuğrul Erdem ^{1*}, Tolga Yılmaz ², Mehmet Kamanlı ³, Ayşe Sefa Tezcan ⁴

¹ Department of Civil Engineering, Manisa Celal Bayar University, Manisa (Türkiye); tugrul.erdem@cbu.edu.tr

² Department of Civil Engineering, Konya Technical University, Konya (Türkiye); tyilmaz@ktun.edu.tr

³ Department of Civil Engineering, Konya Technical University, Konya (Türkiye); mkamanli@ktun.edu.tr

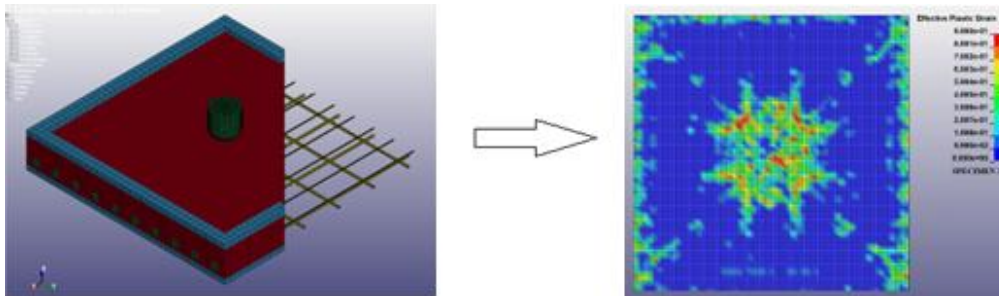
⁴ Department of Civil Engineering, Konya Technical University, Konya (Türkiye); e238222001012@ktun.edu.tr

*Correspondence: tugrul.erdem@cbu.edu.tr

Received: 12.06.25; **Accepted:** 19.02.26; **Published:** 06.03.26

Citation: Erdem, R.T., Yılmaz, T., Kamanlı, M., and Tezcan, A. S. (2026). Numerical evaluation of prestressed concrete slabs subjected to impact loading. *Journal of Construction*, 25(1), 129-148. <https://doi.org/10.7764/RDLC.25.1.129>

Graphical Abstract:



Highlights:

- A validated numerical framework predicts impact response of prestressed slabs.
- The coupled effects of prestress level, strength, and impact energy are quantified.
- Energy absorption and residual deformation govern the impact resistance of slabs.
- The model reproduces damage patterns and failure mechanisms under impact scenarios.

Abstract: Reinforced concrete (RC) structural elements could be exposed to impact loads due to several reasons in their expected service lives. However, impact loading is often overlooked in the design phase of RC elements, unlike quasi-static or other dynamic loads, such as earthquake and wind loads. Because sudden impact loads can cause significant damage to structural systems within a short period, they may result in substantial damage to a structural element or the collapse of the entire structure. Structural engineers tend to investigate the effects of impact loads both experimentally and numerically. This study aims to determine the dynamic responses and failure modes of prestressed concrete slabs. For this purpose, an improved finite element analysis that incorporates prestress effect and strain-rate effects for concrete and steel materials has been developed to investigate the impact behavior of prestressed concrete slabs. To validate the finite element analysis, maximum impact force and displacement values, as well as the residual displacements and energy absorption

capacities of the two specimens, were compared with the experimental results reported in a previous study. Subsequently, a parametric study was conducted using different analysis inputs, and the results were evaluated at the end.

Keywords: Dynamic behavior, finite element analysis, impact load, prestressed concrete plates, LS-DYNA.

List of abbreviations:

FEM: Finite elements model
RC: Reinforced concrete
 ΔL_c : Shortening of the concrete element
 ΔL_{Te} : Elongation of the tendon element
 ΔL_T : Shortening of the tendon when the temperature drops without contact force
 ΔT : Change of temperature
 α : Thermal expansion coefficient of tendons
 ε_c : Strain of the concrete
 ε_{Te} : Strain of the tendon
 ε_T : Strain of the tendon due to temperature drops without any restraints
f: Prestressing force
 A_c : Cross-sectional area of concrete block
 E_c : Elastic modulus of concrete
 A_s : Cross-sectional area of a tendon
 E_s : Elastic modulus of tendon
DIF_t: Tensile dynamic increase factor for concrete
DIF_c: Compression dynamic increase factor for concrete
 $f'_{t,d}$: Dynamic tensile strength
 f'_t : Static tensile strength
 $f'_{c,d}$: Dynamic compressive strength
 f'_c : Static compressive strength
 $\dot{\varepsilon}$: Effective strain rate
 η_t : Fluidity parameters in uniaxial tensile stress
 η_s : Fluidity parameters in shear stress
 η_c : Fluidity parameters in uniaxial compressive stress
 η_{0t} : Rate effect parameter for uniaxial tensile stress
 η_{0c} : Rate effect parameter for uniaxial compressive stress
 N_t : Rate effect power for uniaxial tensile stress
 N_c : Rate effect power for uniaxial compressive stress
DIF_{st}: Tensile and compression dynamic increase factor for steel
 f_y : Yield strength of steel

1. Introduction

Prestressed concrete is a widely used construction material that enhances the performance of structural elements by introducing internal compressive forces before the application of external loads. This is typically achieved through pre-tensioning or post-tensioning, in which high-strength steel tendons are tensioned and anchored to compress the concrete. The primary

advantage of prestressed concrete lies in its ability to counteract tensile stresses, thereby reducing or eliminating cracking under service loads. As a result, it offers improved durability, higher load-carrying capacity, and longer spans with reduced cross-sectional dimensions compared to conventional reinforced concrete (Hassan et al., 2021; Iqbal et al., 2019). Prestressed concrete is commonly employed in bridges, high-rise buildings, parking structures, and other infrastructure where enhanced structural efficiency, crack control, and serviceability are critical (Bai, 2019; Li et al., 2024). Its use also contributes to material savings and architectural flexibility, making it a preferred choice in modern civil engineering applications.

Reinforced concrete (RC) plates are essential structural elements that distribute loads across a surface and efficiently transfer them to supporting members, such as beams, columns, or shear walls (MacGregor and Wight, 2012). Commonly employed in floor systems, RC plates play a vital role in ensuring structural integrity, serviceability, and occupant comfort. Their design must account for various types of loading, including dead loads, live loads, and in some cases, seismic and wind loads. Due to their two-dimensional load-carrying behavior, RC plates resist bending moments and shear forces in multiple directions, offering enhanced structural redundancy and stability. RC plates also help to distribute lateral forces and maintain overall rigidity in a structural system. Proper reinforcement detailing is crucial for controlling cracking, limiting deflections, and ensuring long-term durability under service conditions. Given their widespread application and functional importance, RC plates are a fundamental component in both traditional and modern reinforced concrete structures (Kwak and Kim, 2002; Wu et al., 2018).

Impact loads are characterized by high intensity and extremely short duration, often resulting from sudden collisions or striking events, such as vehicle impacts, falling objects, dropped weights, or debris from explosions. These loads induce rapid stress waves in structural elements, leading to localized damage, large deformations, or even sudden failure, depending on the severity and location of the impact. Unlike sustained or quasi-static loads, impact loads generate dynamic responses that can significantly exceed those produced by conventional loading scenarios. Despite their potential to cause severe structural damage, impact loads are generally not explicitly addressed in seismic design codes, which primarily focus on ground-motion-induced forces with longer durations and broader, system-wide effects. This omission is partly due to the unpredictability and case-specificity of impact events, as well as the complexity of modeling such dynamic interactions. However, in critical infrastructure or structures exposed to high-risk environments, impact loading is increasingly being considered during design and assessment to ensure resilience and safety.

Researchers have designed impact test setups to observe the responses and behavior of structural elements under impact loading lately (Chen and May, 2009; Chen et al., 2020; Çalışkan et al., 2023; Erdem, 2021; Kumar et al., 2018; Li et al., 2024). However, designing reliable and realistic test setups that accurately simulate impact conditions requires careful planning and specialized expertise. One of the primary difficulties lies in the high cost associated with the manufacture of test specimens, instrumentation, and the acquisition or development of impact-loading devices capable of generating controlled, repeatable forces. Additionally, many testing systems have limited measurement precision, which can restrict the range of impact energy that can be applied. These constraints make large-scale and high-energy impact testing particularly difficult to conduct. As a result, while experimental investigations are essential for observing the impact behavior of test specimens, their practical limitations often necessitate complementary computational approaches to explore a broader range of impact scenarios and structural configurations.

Numerical analysis based on nonlinear finite element analysis (FEA) plays a critical role in investigating the effects of impact loads on structural elements, offering a robust and reliable procedure for simulating complex dynamic behavior that is often difficult to capture through physical testing alone. The FEA enables detailed modeling of material non-linearities, strain-rate effects, progressive damage, and failure mechanisms under high-intensity, short-duration loads. One of its significant advantages is the ability to conduct parametric studies efficiently, allowing researchers and engineers to examine the influence of various factors such as impact energy, location, geometry, and material properties without the high costs and logistical challenges associated with experimental testing. Moreover, validated FEA, developed through comparison with experimental data, can be used with confidence to predict structural performance across a wide range of impact scenarios. These models not only help in extending the findings of limited physical tests but also support the optimization and design of

safer, more resilient structures in both standard and extreme conditions (Erdem and Gücüyen, 2017; Erdem and Gücüyen, 2025; Wang and Guo, 2023; Wang et al., 2022; Yılmaz et al., 2022; Yılmaz et al., 2024).

There are relatively few studies on the impact behavior of prestressed concrete structural elements, owing to the complexity of accurately modeling and testing such systems (Kumar et al., 2018; Wu et al., 2018). Prestressed elements exhibit unique mechanical responses under dynamic loading, influenced by initial prestressing forces, tendon behavior, and potential bond-slip effects, all of which complicate experimental and numerical investigations. Additionally, the high cost and technical challenges of constructing and testing prestressed concrete structural elements under impact conditions have limited research in this area. As a result, despite their widespread use in critical infrastructure, the impact performance of prestressed concrete structural members remains less well explored than that of conventional reinforced concrete (RC) components.

A review of the limited number of studies on prestressed concrete elements in the literature indicates that researchers have most often applied low-velocity impact loads. Cheng et al. (2024) evaluated the performance of FRP-repaired reinforced concrete piers following blast damage. The study concludes that CFRP is more effective than other strengthening alternatives due to its high strength-to-weight ratio and superior energy-absorption capacity. Wang et al. (2022) used LS-DYNA to examine the dynamic response of bonded unidirectional prestressed concrete slabs subjected to low-velocity impact. Findings indicate that prestressing enhances impact stiffness and penetration resistance, thereby reducing overall damage. Al Rawi et al. (2020) investigated post-tensioned concrete slabs subjected to impact loads and compared them with reinforced concrete (RC) slabs. The results demonstrate that post-tensioned slabs have exhibited higher energy absorption and superior structural integrity under dynamic loads. Bai (2019) has explored the blast resistance of prestressed concrete slabs using LS-DYNA simulations.

The study highlights the influence of the degree of prestress and slab thickness on peak displacement and failure modes. Li et al. (2024) examined unbonded prestressed concrete slabs under low-velocity impact loads, discussed energy dissipation mechanisms, and proposed an improved numerical model to predict failure patterns. Iqbal et al. (2019) investigated the impact resistance of prestressed concrete plates using both experimental and numerical methods. The research highlights that prestressed plates exhibit higher impact and reaction forces than non-prestressed plates and experience reduced displacements. Hassan et al. (2021) have used Abaqus software to model prestressed bridge decks subjected to blast loads. The research successfully simulates crack propagation and failure progression, providing insights into strategies to mitigate catastrophic collapse and optimize reinforcement detailing to enhance blast resistance. Wang and Guo (2025) developed a theoretical model for bidirectional bonded prestressed slabs under low-velocity impact. The study provides practical guidelines for designing prestressed slabs with enhanced impact resistance. Zhi et al. (2025) have investigated the curved prestressed concrete shells subjected to low-velocity impact loads. The results reveal that higher prestress levels improve shear resistance, whereas lower curvature increases susceptibility to flexural failure.

The present study investigates the impact response and failure modes of prestressed concrete slabs. Firstly, finite element models (FEM) of prestressed concrete slabs were generated using LS-DYNA, which yields the most accurate results for such solutions (LS-DYNA, 2007). The proposed FEM has been validated using two specimens subjected to a detailed experimental program by Kumar et al. (2018). Subsequently, a nonlinear explicit dynamic analysis is performed for a total of eight specimens, varying the prestressing degree, compressive strength, and input impact energy, as controlled by the drop height of the impact hammer. Maximum impact force, maximum and residual displacement, and energy absorption values have been determined for each specimen. In addition, the effective plastic strain distributions of the specimens are presented visually under impact loading. While prior studies have examined the impact behavior of prestressed concrete elements, the combined influence of prestress level, concrete compressive strength, and impact energy on the nonlinear response and damage evolution of prestressed slabs has not been systematically investigated using a validated numerical model. This study addresses this gap by developing and validating a nonlinear numerical framework capable of accurately reproducing experimental behavior and enabling comprehensive parametric evaluation of key factors governing impact resistance. The proposed model provides a reliable tool for understanding failure mechanisms and improving the assessment and design of prestressed concrete slabs subjected to impact loading.

The remainder of this paper is organized as follows. Section 2 presents the materials and methods, including an overview of the experimental study used for model validation and the properties of the prestressed concrete slabs investigated. Section 3 describes the finite element analysis procedure. Section 4 discusses the numerical results. Finally, Section 5 provides the conclusions and comments.

2. Materials and methods

2.1. Overview of the experimental study used for validation of the present FEA

The experimental study by Kumar et al. (2018), which investigated prestressed concrete plates subjected to impact forces, was used to validate the presented finite element model. For the test, two prestressed concrete plates measuring 800 x 800 x 100 mm were cast. The concrete's 28-day compressive strength was 48.4 MPa. The maximum size of coarse aggregate used for the manufacture of the prestressed concrete slabs was 10 mm. Besides, natural sand was used as fine aggregate. The Ordinary Portland Cement of 43 grade has been used for the concrete mix. The ratio of concrete mix ingredients was 1:1.74:1.68 (cement/fine aggregate/coarse aggregate). The prestressed concrete slab was designed using high-yield deformed steel rebars. The diameter of the steel bars was 8 mm. The steel rebars were spaced at 140 mm in the two directions of the prestressed concrete. The average yield strength of the rebars was determined to be 609 MPa following a uniaxial tension test. In prestressed concrete plates, 10 prestressing wires of diameter 4 mm were provided at a center-to-center spacing of 80 mm, with an eccentricity of 25 mm from the center of the plate thickness, to achieve the required prestress (10%). The ultimate tensile load-carrying capacity of the prestressing wires, as measured on a Universal Testing Machine, was 20.5 kN.

In the experimental program, the prestressed concrete slabs tested under impact loading were subjected to fixed boundary conditions. The rotations and translations of plate edges were constrained. Impact energy has been applied to the center of the plates by dropping a steel cylinder hammer with a diameter of 100 mm freely. The weight of the hammer was 242.85 kg. The input impact energies transferred to two prestressed concrete slabs are 1.190 kJ and 2.380 kJ, which correspond to hammer drop heights of 500 mm and 1000 mm, respectively. The test setup, geometric dimensions, rebar, and tendon layouts of the prestressed concrete slabs are depicted in Figures 1 and 2, respectively (Kumar et al., 2018). The time histories of the impact load acting on the prestressed concrete plates and the displacements measured at the center point of the plates on the tension side, recorded during tests, have been used to validate the presented finite element analysis (FEA). Furthermore, the impact load-induced crack on the tension side of the two slabs has been compared to damage distributions obtained by the numerical model.

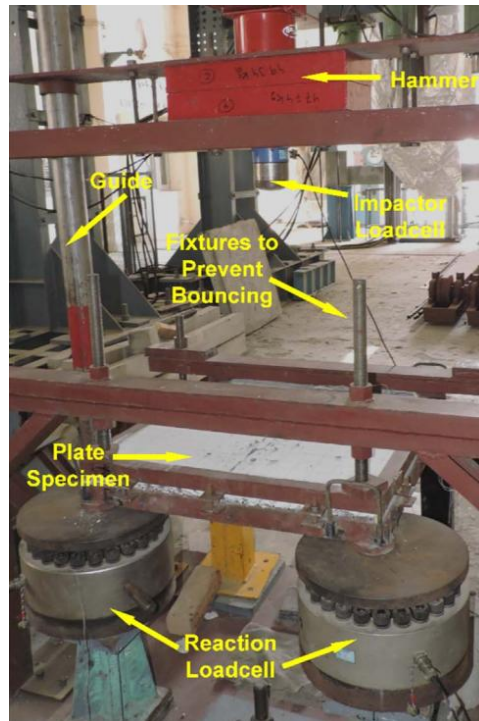


Figure 1. Test setup (Kumar et al., 2018).

2.2. Properties of the prestressed concrete slabs investigated in the present study

Within the scope of the present study, the aim is to investigate the effects of the input impact energy transferred to the prestressed slab during impact loading, as well as the concrete compressive strength and the prestress level applied to the slabs, on the dynamic behavior and failure modes of prestressed slabs subjected to impact loads. Therefore, finite element models of eight square prestressed slabs, each 800 x 800 x 100 mm, were generated. Table 1 presents properties of the prestressed slabs used in numerical analysis. Two of them (S1 and S5) have properties identical to those of plates used in the experimental program conducted by Kumar et al. (2018). These plates were also used to validate the current finite element model and to assess the overall impact behavior of the remaining plates.

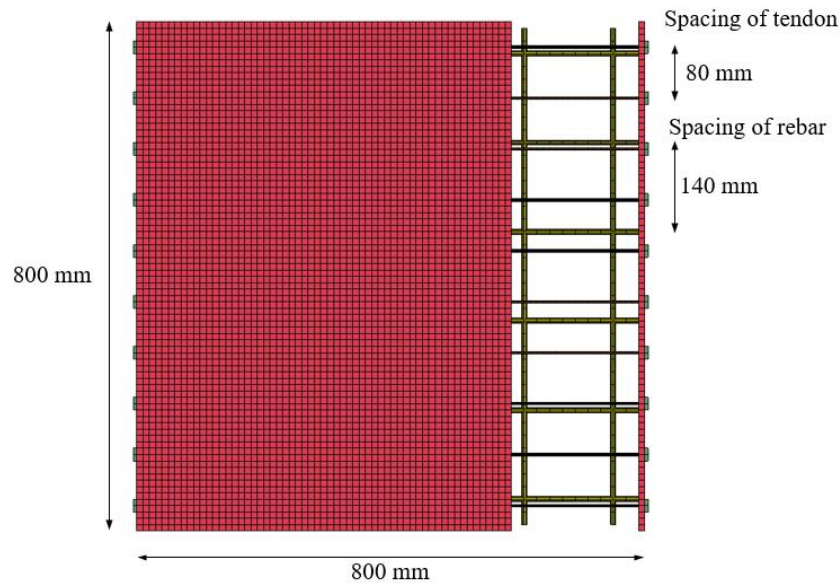


Figure 2. Geometric dimensions, tendon, and rebar layouts.

Table 1. Properties of the prestressed concrete slabs.

Specimen	Prestressing degree (%)	Compressive strength (MPa)	Drop height (m)	Input energy (kJ)
S1	10	48.4	0.5	1.190
S2	5	48.4	0.5	1.190
S3	10	30.0	0.5	1.190
S4	5	30.0	0.5	1.190
S5	10	48.4	1.0	2.380
S6	5	48.4	1.0	2.380
S7	10	30.0	1.0	2.380
S8	5	30.0	1.0	2.380

3. The finite element analysis

The LS-DYNA software has been utilized to generate the finite element model (FEM) of prestressed concrete slabs subjected to impact loading (LS-DYNA, 2007). The LS-DYNA software, which supports explicit dynamic analysis, includes various concrete material models for dynamic loading and enables the use of advanced contact algorithms to simulate the interaction of colliding parts during impact analysis (Şengel et al., 2022a; Şengel et al., 2022b).

The implementation of temperature-induced shrinkage is a well-established numerical technique for introducing prestress forces in tendon elements (Do et al., 2018). In this approach, the *DYNAMIC RELAXATION (DR) option is employed to initialize the prestressed state prior to impact loading. During the DR phase, the prestress-induced distortional kinetic energy is monitored, and convergence is achieved once the ratio of the current to peak kinetic energy falls below a prescribed tolerance. In the present study, a convergence tolerance of 10^{-5} and 5% concrete damping were adopted to ensure numerical stability. After convergence, the stabilized prestressed state is automatically transferred to the subsequent explicit transient analysis.

The prestressing tendons were modeled using the *MAT_ELASTIC_PLASTIC_THERMAL (MAT_004) material card in conjunction with the *LOAD_THERMAL_LOAD_CURVE keyword to prescribe time-dependent temperature histories. Two temperature–time curves were defined: the first applies a rapid temperature drop during the dynamic relaxation phase to generate the target prestress force, while the second maintains a constant temperature throughout the explicit impact analysis, as illustrated in Figure 3.

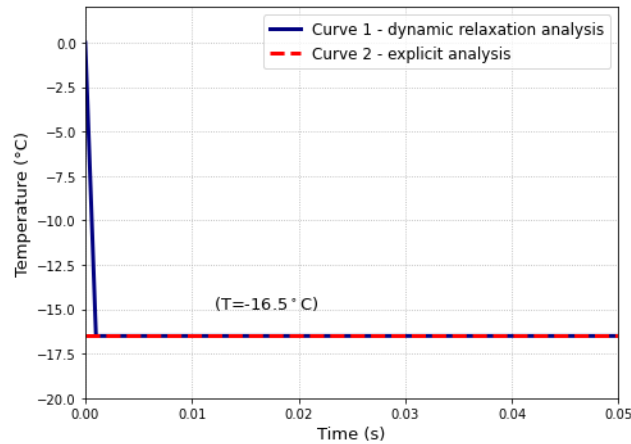


Figure 3. Temperature-time curves.

When the slab cross-section was divided into ten segments, each concrete block contained a centrally located tendon (Figure 4). The prestress force was transferred to the surrounding concrete through anchor plates connected using the *AUTOMATIC_SURFACE_TO_SURFACE contact algorithm. As the tendon was shortened due to the imposed temperature decrease, a tensile force was generated in the tendon and a corresponding compressive force was induced in the concrete block. The compatibility of deformations between the concrete and the tendon can be expressed as (Do et al., 2018):

$$\Delta L_c + \Delta L_{Te} = \Delta L_T \quad (1)$$

which leads to the strain compatibility condition:

$$\varepsilon_c + \varepsilon_{Te} = \varepsilon_T \text{ or } \frac{f}{A_c E_c} + \frac{f}{A_s E_s} = \Delta T \times \alpha \quad (2)$$

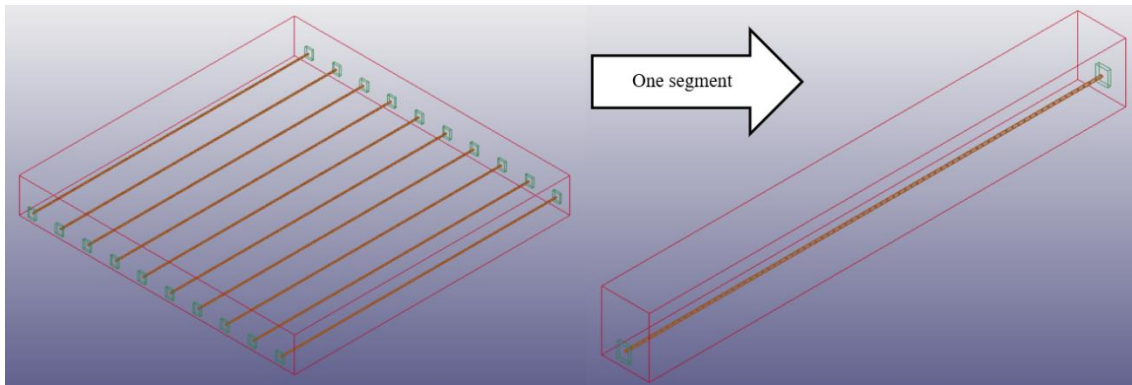


Figure 4. Concrete block and tendon.

Accordingly, the temperature drop required to achieve the target prestress force can be calculated as (Do et al., 2018):

$$\Delta T = \frac{f}{\alpha} \left(\frac{1}{A_c E_c} + \frac{1}{A_s E_s} \right) \quad (3)$$

In the present study, a thermal expansion coefficient of $\alpha = 5 \times 10^{-4} \text{ } ^\circ\text{C}^{-1}$ was defined for the tendons, and a uniform temperature drop was applied to achieve a prestress level corresponding to 10% of the tendon tensile strength. Using $F = 20.5$

kN, $E_c = 32$ GPa, $E_s = 200$ GPa, $A_c = 0.08 \times 0.10$ m², and $A_s = \pi(4 \text{ mm})^2/4$, the required temperature drop was calculated as $\Delta T \approx -16.5$ °C.

It is emphasized that the imposed temperature field was employed solely as a numerical technique to generate the desired initial prestressing force (i.e., fictitious thermal strain) rather than to represent a physical thermal process. Therefore, temperature-dependent mechanical properties beyond the thermal expansion coefficient were not activated for the tendons, and their response during impact loading was governed by the elastic–plastic constitutive behavior under ambient conditions, while the temperature field was applied exclusively to the tendon elements.

The generated FEM comprises the RC slab, steel rebars, tendons, support, and hammer parts. While an 8-node hexahedron solid element was used for modeling the concrete, support, and hammer, the steel rebars and tendons were modeled with a Hughes-Liu beam element (Şengel et al., 2022a; Şengel et al., 2022b). The finite element model of Specimen 1 is given in Figure 5 as an example. After mesh convergence trials, it has been found that the element sizes of support, rebar, concrete, anchor, tendon, and hammer, set at 20 mm, 20 mm, 10 mm, 10 mm, 10 mm, and 5 mm, respectively, provide the optimum results, considering both accurate responses and computational time. Impact load was applied by specifying the hammer's velocity at the moment of collision. Frictional losses in the steel weight's drop were neglected.

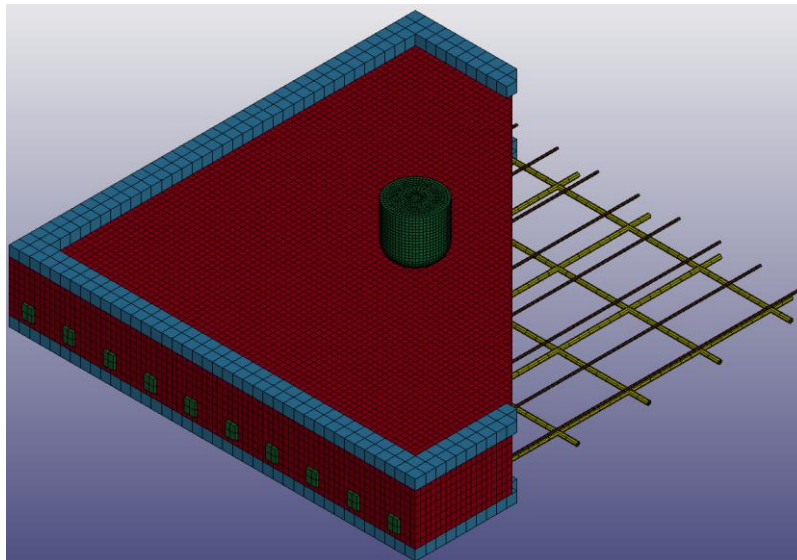


Figure 5. Finite element model of specimen 1.

The concrete material was modeled using the 159-CSCM concrete (Continuous Surface Cap Model), which is based on isotropic constitutive equations and includes a continuous yield surface formulated in terms of three stress invariants of the deviatoric stress tensor. The nonlinear constitutive behavior of concrete was represented using the CSCM (MAT_159), which inherently accounts for plasticity, damage accumulation, stiffness degradation, and strain softening under both tensile and compressive loading. In this model, the uniaxial stress–strain relationships in tension and compression are internally generated from the specified unconfined compressive strength, aggregate size, and density, using experimentally calibrated failure and hardening–softening surfaces. Crack initiation, propagation, and crushing are governed by the evolution of a damage parameter that ranges from 0 (undamaged) to 1 (fully damaged), enabling realistic simulation of the nonlinear response under impact loading (Xiao and Fujikake, 2017).

Once the damage parameter reaches unity, element erosion is activated, and severely damaged concrete is removed from the solution to prevent numerical instability. In the CSCM concrete model, the nonlinear stress–strain behavior is implicitly

defined by internally generated shear and cap yield surfaces, together with triaxial compression and tension meridians; therefore, explicit user-defined stress–strain curves or yield-surface plots are not required. Detailed properties of the CSCM model are provided in the user’s manual (Murray, 2007). The CSCM model requires only three parameters to define concrete behavior: the unconfined compressive strength, maximum aggregate size, and density. In the present study, the cylinder compressive strength was taken as 40.8 MPa, using a conversion factor of 0.84, while the maximum aggregate size and concrete density were set at 10 mm and 2400 kg/m³, respectively.

Steel reinforcement was modeled as an elastic–plastic material without hardening using the *MAT_PIECEWISE_LINEAR_PLASTICITY (MAT_24) model. The steel yield strength and elastic modulus of the longitudinal reinforcement were defined as 609 MPa and 200 GPa, respectively. Poisson’s ratio and density were taken as 0.3 and 7850 kg/m³. The strain-rate sensitivity of steel was incorporated via dynamic increase factor (DIF) curves, thereby enhancing material strength under high-rate loading conditions and ensuring accurate representation of nonlinear steel behavior during impact events. Prestressing tendons were modeled using the *MAT_ELASTIC_PLASTIC_THERMAL (MAT_004) material model, in which prestressing force was introduced through temperature-induced strain. The relationship between material properties and temperature was defined using time-dependent thermal loading curves applied during the dynamic relaxation and explicit analysis phases via the *LOAD_THERMAL_LOAD_CURVE keyword. The hammer and supports were modeled as rigid materials.

In the present finite element model, the interaction between concrete and steel reinforcement/prestressing tendons was represented using a perfect-bond assumption, in which the steel elements were fully embedded in the surrounding concrete, with no relative slip at the interface. This approach is commonly adopted in impact simulations that focus on the global dynamic response, in which inertia effects, strain-rate sensitivity, and overall stiffness dominate the structural behavior. Although bond–slip effects may influence local stress transfer mechanisms and crack development at the steel–concrete interface, experimental and numerical studies have demonstrated that under high-rate loading conditions the apparent bond strength between steel reinforcement and concrete increases, while the development of interfacial slip and associated cracking is restrained due to inertia and confinement effects (Long et al., 2020; Long et al., 2024; Dey et al., 2022). Accordingly, the perfect bond assumption provides a reasonable approximation for capturing the overall dynamic response and dominant failure modes of the slabs investigated in this study. Nevertheless, explicit modeling of bond–slip behavior could further refine local damage predictions, particularly with respect to crack spacing and reinforcement stress distribution and may be considered in future studies.

To verify that the prestressing force was correctly transferred from the tendons to the surrounding concrete, the concrete stress distribution was examined immediately after completion of the dynamic relaxation phase and prior to impact loading. Figure 6 presents the longitudinal normal stress (σ_x) contours of specimen S1 at this stage. The results show compressive stresses concentrated in the bottom region of the slab in the vicinity of the tendons, while only slight tensile stresses are observed near the top surface. This stress distribution is fully consistent with the expected initial stress state of a prestressed concrete slab and confirms that the prestressing force was effectively transmitted from the tendons to the concrete through the anchorage system. Accordingly, the initial stress state adopted in the subsequent impact simulations is physically consistent and representative of the prestressed condition.

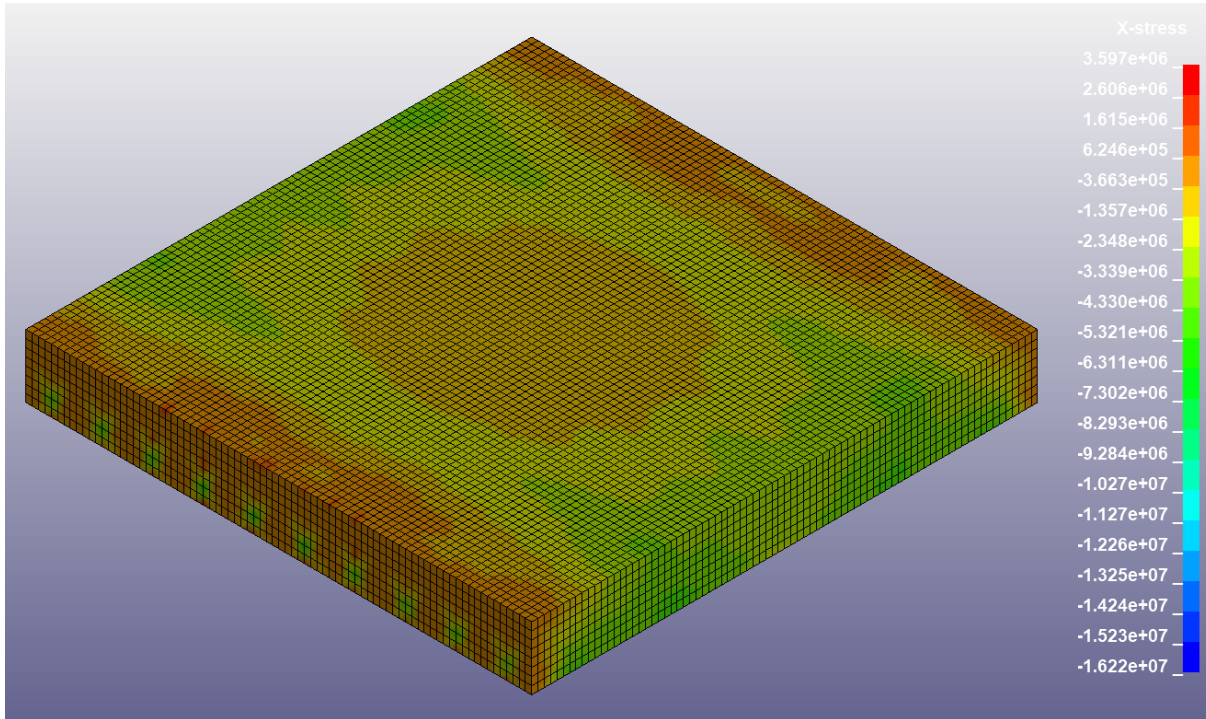


Figure 6. Concrete stress distribution induced by prestressing tendons before impact loading.

Impulsive loading enhances the tensile and compressive strength of steel and concrete materials. This phenomenon is known as a strain-rate effect; its consideration in impact analysis is compulsory for properly evaluating dynamic responses (Bischoff and Perry, 1991; Zhang et al., 2015). This effect is commonly implemented in material models using a Dynamic Increase Factor (DIF), defined as the ratio of dynamic to static strength. Several equations have been presented in the literature to define the DIFs of steel and concrete materials (Malvar and Ross, 1998; Malvar, 1998; Malvar and Crawford, 1998; Fan et al., 2011; Hao and Hao, 2014). For the CSCM model, tensile (DIF_t) and compression (DIF_c) dynamic increase factors can be expressed as follows (Guo et al., 2017):

$$DIF_t = \frac{f'_{t,d}}{f'_t} = 1 + \frac{E_c \dot{\epsilon} \eta_t}{f'_t} = 1 + \frac{E_c \dot{\epsilon} \eta_{0t}}{f'_t \dot{\epsilon} N_t} \quad (4)$$

$$DIF_c = \frac{f'_{c,d}}{f'_c} = 1 + \frac{E_c \dot{\epsilon} \eta_c}{f'_c} = 1 + \frac{E_c \dot{\epsilon} \eta_{0c}}{f'_c \dot{\epsilon} N_c} \quad (5)$$

η_t , η_s , and η_c , which are the fluidity parameters in uniaxial tensile stress, shear stress, and uniaxial compressive stress, can be defined as follows:

$$\eta_t = \frac{\eta_{0t}}{\dot{\epsilon} N_t} \quad (6)$$

$$\eta_c = \frac{\eta_{0c}}{\dot{\epsilon} N_c} \quad (7)$$

$$\eta_s = S_{rate} \eta_{0t} \quad (8)$$

In Eq. (5) and Eq. (6), $f'_{t,d}$ and $f'_{c,d}$ are dynamic tensile and compressive strengths, while f'_t and f'_c denote static tensile and compressive strengths. Where η_{0t} is the rate effect parameter for uniaxial tensile stress; η_{0c} is the rate effect parameter for uniaxial compressive stress. N_t is the rate effect power for uniaxial tensile stress. N_c is the rate effect power for uniaxial compressive stress. $Srate$ is the ratio of effective shear stress to the tensile stress fluidity parameter. The numerical analysis used the 159-CSCM concrete material model's default strain-rate parameters, which were calculated from the compressive strength. Moreover, for a given strain rate $\dot{\epsilon}$, the tensile and compressive DIF_{st} of steel material could be determined via Eq. 10. The k coefficient can be calculated through f_y as follows (Malvar, 1998):

$$DIF_{st} = \left(\frac{\dot{\epsilon}}{10^{-4}} \right)^k \tag{9}$$

$$k = 0.074 - \frac{0.04f_y}{414} \tag{10}$$

DIF_{st} was implemented to *MAT_PIECEWISE_LINEAR_PLASTICITY (MAT_24) by defining a curve based on Eq. 9. Accordingly, the effective stress–strain response of both concrete and steel varies during impact as a function of the instantaneous strain rate and is implicitly generated by the adopted rate-sensitive constitutive models within the relevant strain-rate range, without requiring explicit user-defined stress–strain curves. Translation and rotation DOFs of the steel support were constrained using the *BOUNDARY_SPC_SET keyword. The penalty-based contact algorithm was used for the interface between the hammer and the prestressed slab, as well as for the interface between the support and the prestressed slab via the *AUTOMATIC_SURFACE_TO_SURFACE keyword. Geometric nonlinearity in deformation was inherently accounted for in the present analyses through the explicit dynamic formulation implemented in LS-DYNA. The solver employs an updated Lagrangian approach that allows large element displacements and rotations, as well as nonlinear contact interactions, to be naturally captured during impact events. Therefore, additional geometric stiffness formulations or co-rotational beam elements were not explicitly introduced, as the essential geometric nonlinear effects associated with large deformation behavior are already accounted for in the employed numerical framework.

4. Results and analysis

After completing the non-linear explicit dynamic analysis for each prestressed concrete slab, the outputs are determined from the software. First, numerical results from the present finite element model and experimental data from Kumar et al. (2018) for S1 and S5 slabs were compared to validate the model. The values of peak impact force, peak displacement, residual displacement, and energy absorption for specimens S1 and S5 are given in Table 2. In this table, 'Exp' refers to experimental results, 'Num' refers to numerical analysis results, and 'R' represents the ratio between the two results.

Table 2. Comparison of experimental and numerical values.

Specimen	Peak impact force (kN)			Peak displacement (mm)			Residual displacement (mm)			Energy absorption (J)		
	Exp.	Num.	R	Exp.	Num.	R	Exp.	Num.	R	Exp.	Num.	R
S1	290.8	287.43	1.01	8.2	5.26	1.56	2.68	4.70	0.57	942.52	950.20	0.99
S5	374.9	372.82	1.01	16.09	10.70	1.50	6.97	10.00	0.70	2291.62	2260.58	1.01

Upon examining the experimental and numerical results, it is found that the differences between the experimental and numerical maximum impact forces and energy absorption capacities are only $\pm 1\%$. However, differences between maximum and residual displacements, as numerically and experimentally determined, reach up to 56% and 70%, respectively. The authors consider that, in addition to the pretty good agreement observed between numerical and experimental results for impact forces and energy absorption capacities, the differences in maximum and residual displacements are also within acceptable limits for impact simulations involving very short loading durations. Various factors, such as the nonhomogeneous nature of concrete, challenges in accurately modeling strain-rate effects and material damping, and differences between idealized support conditions in numerical analyses and real supports, which often include frictional motion, can contribute to discrepancies between numerical and experimental findings. Additionally, the complex interactions at contact surfaces during collisions can

further affect these outcomes. Similar levels of acceptable variation in displacements have been reported in other comprehensive numerical studies (Yılmaz and Şengel, 2022; Othman and Marzouk, 2014; Huang et al., 2021; Liu et al., 2020; Batarlar and Saatci, 2022). It should be noted that the relatively large percentage discrepancies observed in maximum and residual displacements are primarily a consequence of the small absolute displacement magnitudes involved. For example, the residual displacement difference in specimen S1 corresponds to an absolute deviation of approximately 2.0 mm, while that of specimen S5 is about 3.0 mm. In the context of impact loading on concrete slabs with span dimensions of 800 mm, such deviations are minor and do not alter the global structural response or the identified failure modes. From a performance-based perspective, the finite element model accurately captures the overall deformation demand, permanent damage level, and energy dissipation characteristics of the slabs. Therefore, although percentage differences in displacement may appear large, their absolute values remain small and have a negligible influence on the interpretation of structural performance and impact resistance.

Based on the validation results, the proposed finite element model (FEM) can be used reliably to predict the impact responses of prestressed concrete slabs. The damage patterns obtained from the numerical simulations are compared with the impact-induced cracks observed in the experimental study, as illustrated in Figure 7. The comparison indicates that the FEM can reproduce the overall damage localization and dominant failure characteristics observed in the tests. It should be noted that the damage comparison presented in Figure 7 is primarily qualitative. The experimental study used for model validation reports damage primarily through visual crack patterns and descriptive observations, without providing measurable crack metrics such as crack length, crack width, crack density, or damaged-area ratios. Consequently, a direct quantitative comparison of crack geometry is not possible based on the available experimental data. Under impact loading, damage in concrete slabs develops rapidly and remains highly localized, which further complicates reliable experimental measurement of crack geometry.

In the present numerical framework, damage severity is therefore assessed using quantitative deformation- and damage-related indicators, including effective plastic strain distributions, residual displacement, and energy absorption capacity. These parameters are directly associated with permanent damage, stiffness degradation, and energy dissipation, and provide an objective, performance-oriented basis for evaluating the finite element model's damage-prediction capability. Accordingly, although the damage comparison is visual, the numerical model exhibits physically consistent agreement with the experimentally observed damage patterns and dominant failure modes. In addition to the qualitative comparison of surface crack patterns, the ability of the numerical model to replicate crack formation and propagation is further assessed through plastic strain contours obtained from the finite element analysis. The spatial distribution and orientation of high plastic strain zones are in good agreement with experimentally observed crack locations and shapes, particularly crack initiation beneath the impact point and subsequent radial and flexural crack propagation. These results indicate that the adopted damage and plasticity formulation captures the dominant failure mechanisms and crack-evolution trends observed in the experiments.

Thereafter, finite element models were also generated for the remaining specimens. Thus, a parametric analysis was performed on eight prestressed concrete plates using an explicit nonlinear dynamic procedure in LS-DYNA. In this parametric study, the effects of concrete compressive strength, degree of prestressing, and input impact energy on the impact behavior of prestressed concrete slabs were systematically investigated. The concrete compressive strength was varied by assigning different strength values in the concrete constitutive model, while the prestressing degree was modified by applying different initial prestress levels to the tendons using the temperature-induced strain approach described previously. The input impact energy was controlled by changing the drop height of the impact hammer, which directly determined the impact velocity and kinetic energy. Each parameter was varied independently while keeping the remaining parameters constant, allowing the isolated influence of each variable on the dynamic response and damage evolution of the slabs to be evaluated. Table 3 summarizes the numerical results of the parametric analysis, including peak impact force, displacement-related response parameters, and corresponding energy-absorption capacities. Time histories of impact force and displacement are presented for better understanding. The specimens have been divided into two groups for each impact energy value. While impact force-time graphs are shown in Figure 8, displacement-time graphs are presented in Figure 9.

After generating time histories of impact force and displacement, impact force-displacement curves were obtained at the same time intervals as those used for the impact force and displacement data. Calculating the area under these curves enables

the determination of energy-absorption values for all prestressed concrete plates, as listed in Table 3. The impact force-displacement curves, which are also generated for each impact energy value, are exhibited in Figure 10.

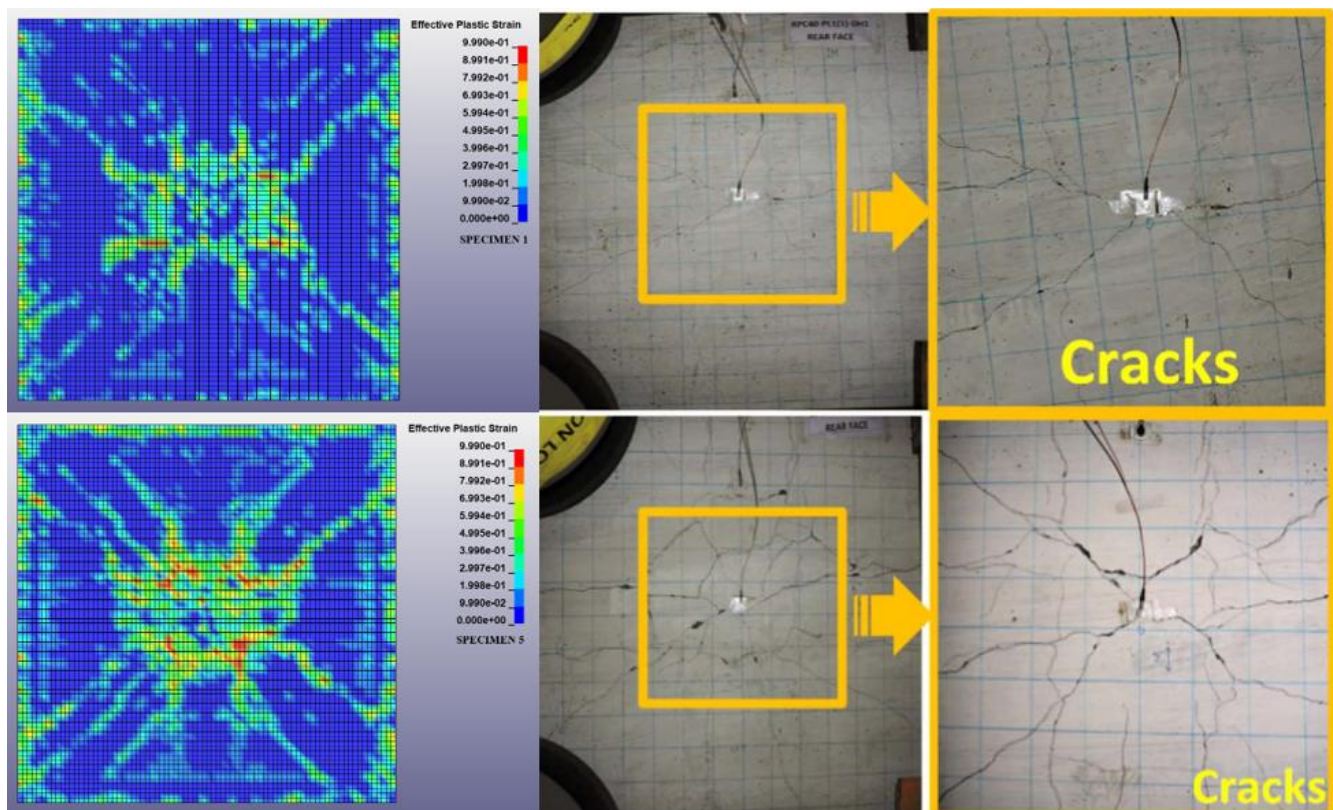


Figure 7. Damage patterns observed in the test and the numerical analysis.

Table 3. Results of the parametric analysis.

Specimen	Peak impact force (kN)	Peak displacement (mm)	Residual displacement (mm)	Energy absorption (J)
S1	287.43	5.26	4.70	950.20
S2	267.49	5.99	5.36	936.42
S3	258.35	8.40	8.11	1180.68
S4	248.02	9.94	9.51	1156.83
S5	372.82	10.70	10.00	2260.58
S6	362.03	11.11	10.55	2270.15
S7	289.57	17.14	17.14	2258.60
S8	274.79	17.44	16.61	2235.38

Results indicate that increasing the prestress force increases stiffness and impact load resistance, resulting in higher maximum impact forces and lower maximum and residual displacements. Furthermore, when higher input impact energy was applied to specimens, the increasing prestress force was less effective in reducing displacements. A similar tendency has been observed in a previous work (Iqbal et al., 2019). Additionally, the increase in prestress force has enhanced the energy-absorption capacity. The effects of prestressing and strain rate are inherently coupled under impact loading. Prestressing modifies the slab's initial stress state by introducing compressive stresses, thereby delaying crack initiation, and increasing global stiffness. As a result, prestressed slabs experience shorter impact durations and lower displacement demands than non-prestressed slabs. This stiffer response leads to higher effective strain rates developing locally in both concrete and reinforcement during impact. Consequently, the strain-rate-dependent enhancement of material strength, quantified by dynamic increase factors (DIFs), is more pronounced in prestressed slabs. In this sense, prestressing does not act independently of strain-rate effects; instead, it indirectly governs the activation and intensity of strain-rate-sensitive material behavior by controlling stiffness,

deformation rate, and contact duration. The coupled action of prestress and strain rate, therefore, plays a key role in defining the dynamic response and damage evolution of slabs subjected to impact loading.

When the concrete compressive strength was reduced from 48.4 MPa to 30 MPa, the impact load-bearing capacity decreased, while the maximum and residual displacements increased significantly. Based on the numerical results reported in Table 3, reducing the concrete strength under identical prestressing degree and input impact energy led to increases of up to approximately 66% in maximum displacement and 77% in residual displacement compared to the reference cases with higher concrete strength. Furthermore, peak impact forces transferred to specimens have decreased with the reduction in stiffness of slabs.

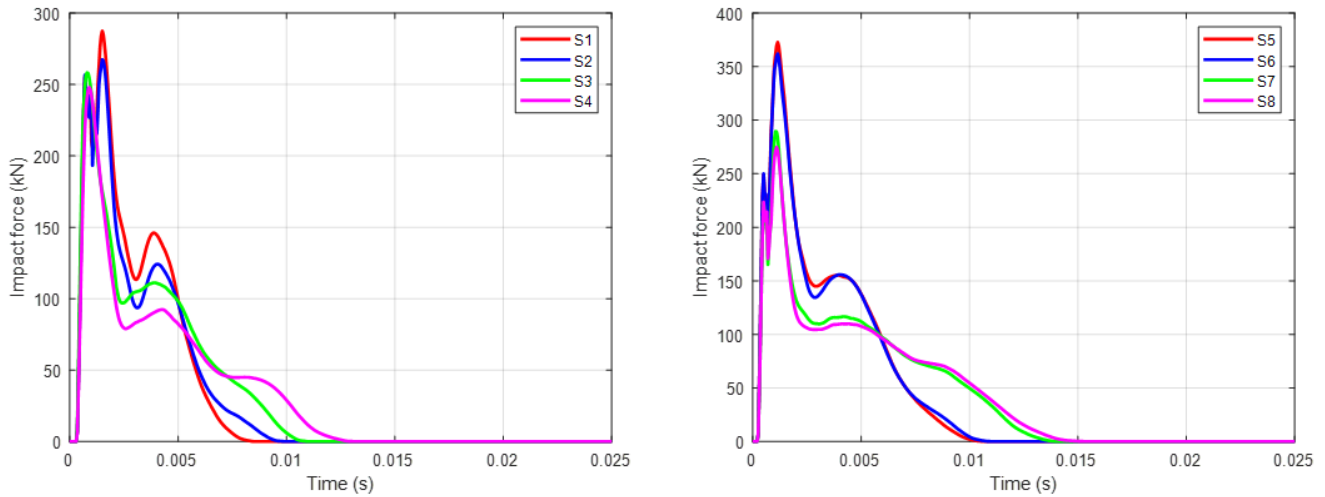


Figure 8. Impact force-time graphs.

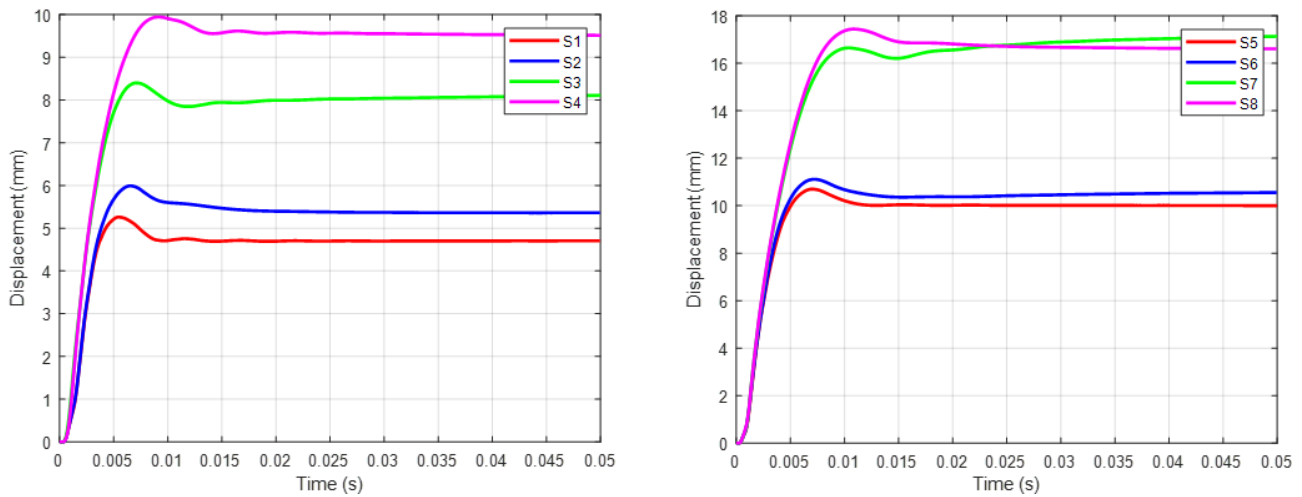


Figure 9. Displacement-time graphs.

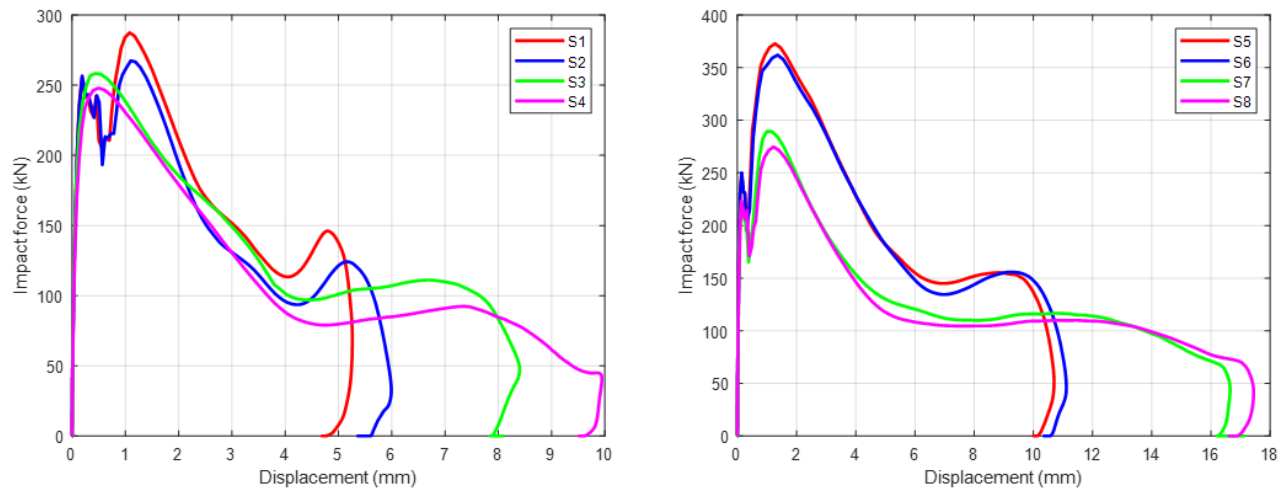


Figure 10. Impact force-displacement curves.

When the input impact energy was doubled by increasing the drop height while keeping the prestressing degree and concrete compressive strength constant, the maximum impact force transmitted to the slabs increased by approximately 35%. Under the same conditions, the maximum and residual displacements increased by up to 2.04 and 2.13 times, respectively. These trends were obtained from direct numerical comparisons of cases with identical material properties and prestressing conditions, as summarized in Table 3. A direct comparison with the corresponding non-prestressed RC slabs reported in the authors' previous study (S1 and S5) clearly quantifies the role of prestressing (Yılmaz and Şengel, 2022). For the 1.190 kJ impact case, the prestressed slabs (S1–S2) exhibited similar peak forces (−2.1% to +5.2%) but markedly lower peak displacements (5.26–5.99 mm vs 10.58 mm; ≈43–50% reduction) and slightly lower residual displacements (4.70–5.36 mm vs 5.51 mm; ≈3–15% reduction) compared to the non-prestressed counterpart. For the 2.380 kJ impact case, the prestressed slabs (S5–S6) again showed comparable peak forces (≈0–3% increase) while substantially reducing peak displacement (10.70–11.11 mm vs 18.99 mm; ≈41–44% reduction) and residual displacement (10.00–10.55 mm vs 14.00 mm; ≈25–29% reduction). These results confirm that prestressing primarily enhances impact stiffness and reduces the permanent deformation demand, leading to more controlled damage evolution compared with conventional RC slabs.

In the final step of the numerical analysis, effective plastic strains were obtained using the software. In this way, possible crack propagation on the tension side of the prestressed concrete slabs can be monitored. Plastic strain values of the specimens are shown in Figure 11. It is observed that fractures accumulate around the midpoint of the specimens where impact loading is applied and then distribute towards the supports. The observed increase in plastic strain levels at higher input impact energies and the more severe damage development in slabs with lower concrete compressive strength were obtained through a systematic parametric analysis. In this analysis, the input impact energy was varied by changing the drop height while maintaining the prestressing degree and concrete compressive strength constant, whereas the effect of concrete strength was evaluated by comparing cases with different compressive strengths under identical prestressing and impact energy conditions. Based on the numerical results summarized in Table 3 and the corresponding effective plastic strain contours, higher input impact energies led to more extensive plastic strain localization and increased damage severity. Similarly, slabs with a concrete compressive strength of 30 MPa exhibited larger plastic strain regions and more pronounced damage compared to slabs with higher concrete strength subjected to the same impact energy and prestressing level. These comparisons isolate the influence of impact energy and concrete strength on damage evolution and provide a clear parametric basis for the reported observations.

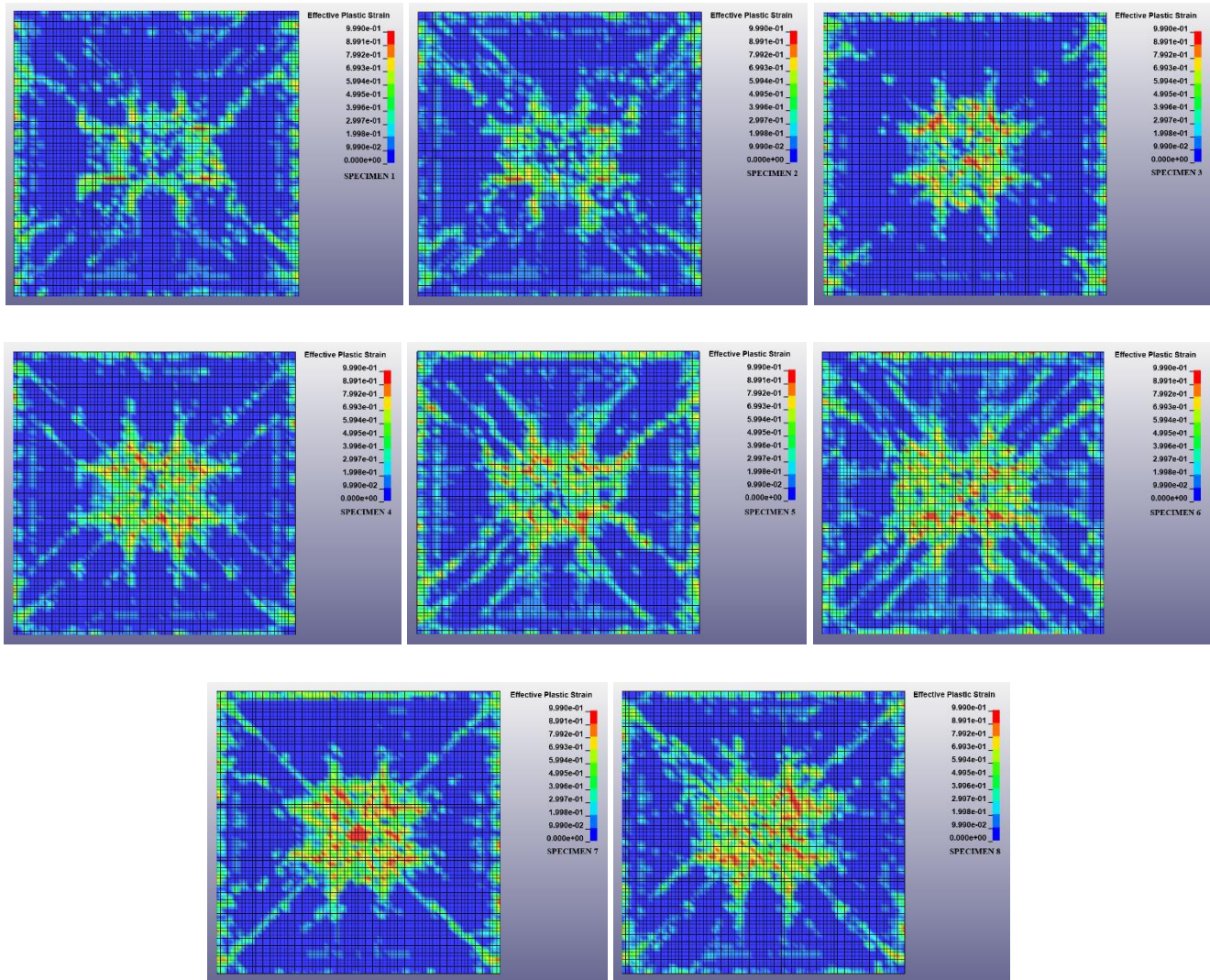


Figure 11. Effective plastic strain contours showing damage patterns of prestressed concrete slabs under impact loading; specimen labels correspond to the numerical cases in Table 3.

5. Conclusions and comments

The present study aims to develop a comprehensive finite element model to investigate the dynamic response and failure modes of prestressed concrete slabs subjected to low-velocity impact loads. First, the present finite element model has been verified against drop-weight test results for two specimens from an experimental program reported in the literature. A parametric study was conducted using the validated finite-element model to investigate the effects of concrete compressive strength, prestress force, and input impact energy on the impact behavior of prestressed concrete slabs. Time-histories of impact load transferred to slabs and maximum and residual displacements measured from slabs are calculated in numerical analysis. Additionally, effective plastic strain has been calculated to assess the damage pattern. Furthermore, the impact behavior of prestressed slabs was analyzed in detail using numerical simulations. Outcomes obtained can be summarized as follows:

1. The experimental results obtained from the study presented by Kumar et al. (2018) and numerical results via the introduced finite element model show excellent agreement in terms of maximum impact force and energy absorption capaci-

ties. There is only a $\pm 1\%$ difference between experimental and numerical results. Moreover, the difference between the maximum and residual displacements obtained from the experiment and numerical analysis is within an acceptable range. Furthermore, the calculated effective plastic strain pattern accurately captures the crack distribution that occurred during the test. The present finite element model has been highly successful in evaluating the impact response and failure modes of prestressed concrete plates.

2. The increase in prestress force has increased stiffness and impact load resistance, resulting in higher maximum impact forces and energy absorption capacities, as well as lower maximum and residual displacements. However, for impact loading with higher input impact energy, the increasing prestress force became less effective in reducing displacements.
3. The decrease in concrete compressive strength, from 48.4 MPa to 30 MPa, resulted in increased maximum and residual displacements measured from the slabs, up to 66% and 77%, respectively.
4. Doubling the input impact energies applied to prestressed concrete slabs increased the maximum impact forces transferred to the slabs by 35%. Additionally, the maximum and residual displacements measured from the slabs increased by 2.04 and 2.13 times, respectively, due to the higher input energy.

Overall, the present study demonstrates that the proposed finite element model can reliably capture the impact behavior of prestressed concrete slabs, as evidenced by the close agreement between experimental observations and numerical predictions. Given the limited number of studies on prestressed concrete members subjected to impact loading, the validated modeling framework provides a useful tool for evaluating the dynamic response of various prestressed concrete elements. Although the present model considers key parameters such as prestress level, concrete compressive strength, and impact energy, certain aspects require further investigation.

Future studies should examine explicit bond–slip interaction between tendons and concrete, alternative prestressing layouts, and the influence of boundary conditions representative of real structural systems. In addition, scale effects, repeated impact scenarios, strain-rate-sensitive material degradation, and long-term deterioration mechanisms such as corrosion should be incorporated to enhance the predictive capability of the model. Extending the framework to different structural configurations and higher impact velocities would also contribute to a more comprehensive understanding of impact-resistant prestressed systems. From a broader perspective, the findings of this study enhance the understanding of impact-resistant prestressed concrete systems and may support the development of performance-based design strategies for resilient structural applications.

Author contributions: Erdem, R. T. has evaluated the analysis results and designed the manuscript. Kamanli, M., has participated in the planning, and writing of the manuscript. Yılmaz, T., and Tezcan, A. S. have performed non-linear explicit dynamic analysis.

Funding: This study is not financially supported.

Acknowledgments: The results of the present study are based on a section of a seminar study of M.Sc(c). Ayşe Sefa Tezcan supervised by Assoc. Prof. Dr. Tolga Yılmaz. The seminar study is conducted during the Master of Science program at the Graduate Education Institute, Konya Technical University.

Conflicts of interest: There is no conflict of interest.

References

- Al Rawi, Y., Temsah, Y., Baalbaki, O., Jahami, A., and Darwiche M. (2020). Experimental investigation on the effect of impact loading on behavior of post-tensioned concrete slabs. *Journal of Building Engineering*, 31, 101207. <https://doi.org/10.1016/j.jobbe.2020.101207>
- Bai, C. (2019). Analysis on dynamic response of prestressed concrete slab subjected to blast loading. *E3S Web of Conferences*, 136, 03015. <https://doi.org/10.1051/e3sconf/201913603015>
- Batarlar B, Saatci S (2022). Numerical investigation on the behavior of reinforced concrete slabs strengthened with carbon fiber textile reinforcement under impact loads. *Structures*, 41, 1164–1177. <https://doi.org/10.1016/j.istruc.2022.05.057>

- Bischoff, P. H., and Perry, S. H. (1991). Compressive behaviour of concrete at high strain rates. *Materials and Structures*, 24(6), 425–450. <https://doi.org/10.1007/BF02472016>
- Chen, Y., and May I. M. (2009). Reinforced concrete members under drop-weight impacts. *Proceedings of the Institution of Civil Engineers – Structures and Buildings*, 162(1), 45-56. <https://doi.org/10.1680/stbu.2009.162.1.45>
- Chen, W., Pham, T. M., Elchalakani, M., Li, H., Hao, H., and Chen, L. (2020). Experimental and numerical study of basalt frp strip strengthened rc slabs under impact loads. *International Journal of Structural Stability and Dynamics*, 20(6), 2040001. <https://doi.org/10.1142/S0219455420400015>
- Cheng, Y. H., Xu, J. P., and Wu H. (2024). Seismic performance of frp-repaired rc piers after blast loading. *Engineering Structures*, 321, 118989. <https://doi.org/10.1016/j.engstruct.2024.118989>
- Çalışkan, Ö., Aras, M., Yılmaz, T., Anil, Ö. and Erdem, R. T. (2023). Impact behavior of low strength concrete slab strengthened with fan type anchored carbon fiber-reinforced polymer strips. *Structural Concrete*, 24, 1689-1711. <https://doi.org/10.1002/suco.202200256>
- Dey, A., Valiukas, D., Jakubovskis, R., Sokolov, A. and Kaklauskas, G. (2022). Experimental and numerical investigation of bond–slip behavior of high-strength reinforced concrete at service load. *Materials*, 15, 293. <https://doi.org/10.3390/ma15010293>
- Do, T. V., Pham, T. M., and Hao, H. (2018). Numerical modelling of prestressed concrete beams subjected to impact loading. *Engineering Structures*, 162, 1–15. <https://doi.org/10.1016/j.engstruct.2018.02.001>
- Erdem, R. T. (2021). Dynamic responses of reinforced concrete slabs under sudden impact loading. *Revista de la Construcción*, 20(2), 346-358. <http://dx.doi.org/10.7764/rdlc.20.2.346>
- Erdem, R. T., and Gücüyen, E. (2017). Non-linear analysis of reinforced concrete slabs under impact effect. *Gradjevinar*, 69(6), 479-487. <https://doi.org/10.14256/JCE.1557.2016>
- Erdem, R. T., and Gücüyen, E. (2025). Impact loading on RC cantilever beam. *Comptes Rendus de l'Academie Bulgare des Sciences*, 78(3), 410-418. <https://doi.org/10.7546/CRABS.2025.03.11>
- Fan, W., Yuan, W., Yang, Z., Fan, Q. (2011). Dynamic demand of bridge structure subjected to vessel impact using simplified interaction model. *Journal of Bridge Engineering*, 16(1), 117–126. [https://doi.org/10.1061/\(ASCE\)BE.1943-5592.000013](https://doi.org/10.1061/(ASCE)BE.1943-5592.000013)
- Guo, W., Fan, W., Shao, X., Shen, D., and Chen, B. (2018). Constitutive model of ultra-high-performance fiber-reinforced concrete for low-velocity impact simulations. *Composite Structures*, 185(November 2017), 307–326. <https://doi.org/10.1016/j.compstruct.2017.11.022>
- Hao Y, Hao H (2014) Influence of the concrete DIF model on the numerical predictions of RC wall responses to blast loadings. *Engineering Structures* 73:24-38. <https://doi.org/10.1016/j.engstruct.2014.04.042>
- Hassan, J.F., Abdul Rahman, A. A., Al-Tarafany, D. M. (2021). Prestressed bridge deck responses to blast loads. *IOP Conference Series: Materials Science and Engineering*, 1067, 012003. <https://doi.org/10.1088/1757-899X/1067/1/012003>
- Huang Z, Chen W, Tran TT, Pham TM, Hao H, Chen Z, Elchalakani M (2021). Experimental and numerical study on concrete beams reinforced with Basalt FRP bars under static and impact loads. *Composite Structures*, 263, 113648. <https://doi.org/10.1016/j.compstruct.2021.113648>
- Iqbal, M. A., Kumar, V., and Mittal, A. K. (2019). Experimental and numerical studies on the drop impact resistance of prestressed concrete plates. *International Journal of Impact Engineering*, 123, 98-117. <https://doi.org/10.1016/j.ijimpeng.2018.09.013>
- Kumar, V., Iqbal, M. A., and Mittal, A. K. (2018). Experimental investigation of prestressed and reinforced concrete plates under falling weight impactor. *Thin-Walled Structures*, 126, 106-116. <http://dx.doi.org/10.1016/j.tws.2017.06.028>
- Kwak, H. G., and Kim, S. P. (2002). Nonlinear analysis of reinforced concrete slabs subjected to lateral loads. *Engineering Structures*, 24(9), 1159–1171. [https://doi.org/10.1016/S0141-0296\(02\)00045-1](https://doi.org/10.1016/S0141-0296(02)00045-1)
- Li, C., Zhi, X., Song, M., Lan, C., and Li S. (2024). Behavior of unbonded prestressed concrete slabs subjected to low-velocity impact loading. *Engineering Structures*, 308, 118006. <https://doi.org/10.1016/j.engstruct.2024.118006>
- Liu B, Fan W, Huang X, Shao X, Kang L (2020). A simplified method to predict damage of axially-loaded circular RC columns under lateral impact loading. *International Journal of Concrete Structures and Materials*, 14(32), 1–24. <https://doi.org/10.1186/s40069-020-00406-z>
- Long, X., Li, H., Iyela, P. M. and Kang, S. B. (2024). Predicting the bond stress–slip behavior of steel reinforcement in concrete under static and dynamic loadings by finite element, deep learning and analytical methods. *Engineering Failure Analysis*, 161, 108312. <https://doi.org/10.1016/j.eng-failanal.2024.108312>
- Long, X., Wang, C. Y., Zhao, P. Z. and Kang, S. B. (2020). Bond strength of steel reinforcement under different loading rates. *Construction and Building Materials*, 238, 117749. <https://doi.org/10.1016/j.conbuildmat.2019.117749>
- LS-DYNA (2007). Keyword user’s manual. Livermore Software Technology Corporation.
- MacGregor, J. G., and Wight, J. K. (2012). *Reinforced concrete: Mechanics and design* (6th ed.). Pearson Education.
- Malvar LJ. Review of static and dynamic properties of steel reinforcing bars. *ACI Mater J* 1998:95. <https://doi.org/10.14359/418>

- Malvar LJ, Ross CA. Review of strain rate effects for concrete in tension. *ACI Mater J* 1998;95. <https://doi.org/10.14359/403>
- Malvar L.J., Crawford J.E., Dynamic increase factors for concrete, DTIC Document, 1998.
- Murray YD. Users manual for LS-DYNA concrete material model 159. United States. Federal Highway Administration. Office of Research; 2007.
- Othman, H., and Marzouk, H. (2014). Numerical investigation of reinforced concrete slabs under impact loading. *Proceedings of the 10th Fib International PhD Symposium in Civil Engineering, Canada.*
- Şengel, S., Erol, H., Yılmaz, T., and Anıl, Ö. (2022a). Investigation of the effects of impactor geometry on impact behavior of reinforced concrete slabs. *Engineering Structures*, 263(March), 114429. <https://doi.org/10.1016/j.engstruct.2022.114429>
- Şengel, S., H., Erol, H., Yılmaz, T., Anıl, Ö., Can Gürdal, H., and Muhammed Uludoğan, A. (2022b). Low-velocity impact behavior of two-way RC slab strengthening with carbon TRM strips. *Structures*, 44, 1695–1714. <https://doi.org/10.1016/j.istruc.2022.08.108>
- Thai, D. K., and Kim, S. E. (2017). Numerical simulation of pre-stressed concrete slab subjected to moderate velocity impact loading. *Engineering Failure Analysis*, 79, 820-835. <http://dx.doi.org/10.1016/j.engfailanal.2017.05.020>
- Wang, Z., Hou, C. and Guo, Q. (2022). Numerical simulation on the dynamic response of bonded unidirectional prestressed concrete slabs subjected to low-velocity impact. *Structures*, 38, 1098-1110. <https://doi.org/10.1016/j.istruc.2022.02.056>
- Wang, Z., and Guo, Q. (2023). Experimental and numerical study on the dynamic behavior of prestressed concrete panels suffering low speed impact. *Structures*, 61, 106043. <https://doi.org/10.1016/j.istruc.2024.106043>
- Wang, Z., and Guo, Q. (2025). Prestressed concrete slabs subjected to low-velocity impact: Theoretical analysis model and design method. *Engineering Failure Analysis*, 167, 108949. <https://doi.org/10.1016/j.engfailanal.2024.108949>
- Wu, Y., Li, Q., and Hao, H. (2018). Numerical investigation of reinforced concrete slabs subjected to impact loading. *Engineering Structures*, 163, 149–162. <https://doi.org/10.1016/j.engstruct.2018.02.048>
- Xiao, Y., Li, B., and Fujikake, K. (2017). Behavior of reinforced concrete slabs under low-velocity impact. *ACI Structural Journal*, 114(3), 643–658. <https://doi.org/10.14359/51689565>
- Yılmaz, T., Şengel, H. S., (2022). Numerical evaluation of reinforced concrete slabs with fixed support under impact load. *Challenge Journal of Structural Mechanics* 8(3), 122–132. <https://doi.org/10.20528/cjsmec.2022.03.005>
- Yılmaz, T., Anıl, Ö. and Erdem, R. T. (2022). Experimental and numerical investigation of impact behavior of rc slab with different opening size and layout. *Structures*, 35, 818-832. <https://doi.org/10.1016/j.istruc.2021.11.057>
- Yılmaz, T., Erdem, R. T., Kishi, N., and Anıl, Ö. (2024). Investigation of impact behavior of shear deficient rc beams using nonlinear fea. *Mechanics Based Design of Structures and Machines*, 52(2), 848-866. <https://doi.org/10.1080/15397734.2022.2124173>
- Zhi, X., Li, C., Song, M., Huang, B., and Fan F. (2025). Experimental and numerical studies on low velocity impact behaviors of curved prestressed concrete shells. *Engineering Structures*, 325, 119412. <https://doi.org/10.1016/j.engstruct.2024.119412>
- Zhang, X., Hao, H., and Li, J. (2015). Experimental investigation of the strain-rate effect on the mechanical properties of concrete subjected to dynamic compression. *Construction and Building Materials*, 82, 28–37. <https://doi.org/10.1016/j.conbuildmat.2015.02.019>



Copyright (c) 2026 Erdem, R.T., Yılmaz, T., Kamanlı, M., and Tezcan, A. S. This work is licensed under a [Creative Commons Attribution-NonCommercial-No Derivatives 4.0 International License](https://creativecommons.org/licenses/by-nc-nd/4.0/).